CHEMISTRY
A EUROPEAN JOURNAL

DOI: 10.1002/chem.200903210

Self-Assembly of Imidazolium-Based Rodlike Ionic Liquid Crystals: Transition from Lamellar to Micellar Organization

Xiaohong Cheng,*[a] Xueqing Bai,[a] Shan Jing,[a] Helgard Ebert,[b] Marko Prehm,[b] and Carsten Tschierske*[b]

Abstract: By using aryl-amination chemistry, a series of rodlike 1-phenyl-1*H*-imidazole-based liquid crystals (LCs) and related imidazolium-based ionic liquid crystals (ILCs) has been prepared. The number and length of the C-terminal chains (at the non-charged end of the rodlike core) and the length of the N-terminal chain (on the imidazolium unit in the ILCs) were modified and the influence of these structural parameters on the mode of self-assembly in LC phases was investigated by polarizing microscopy, differential scanning calorimetry, and X-ray diffraction. For the single-chain imidazole derivatives nematic phases (N) and bilayer SmA_2 phases were found, but upon increasing the number of alkyl chains the LC phases were lost. For the related imidazolium salts LC phases were preserved upon increasing the number and length of the C-terminal chains and in this series it leads to the phase sequence SmA–columnar (Col)–micellar cubic (Cub_I/*Pm*3*n*). Elongation of the N-terminal chain gives the reversed sequence. Short N-terminal chains prefer an end-to-end packing of the mesogens in which these chains are separated from the C-terminal chains. Elongation of the N-terminal chain leads to a mixing of N- and C-terminal chains, which is accompanied by complete intercalation of the aromatic cores. In the smectic phases this gives rise to a transition from bilayer (SmA_2) to monolayer smectic (SmA) phases. For the columnar and cubic phases the segregated end-to-end packing leads to core–shell aggregates. In this case, elongation of the N-terminal chains distorts core–shell formation and removes Cub_I and Col phases in favor of single-layer SmA phases. Hence, by tailoring the length of the N-terminal chain, a crossover from taper-shaped to polycatenar LC tectons was achieved, which provides a powerful tool for control of self-assembly in ILCs.

Keywords: cubic phases · imidazolium salts · ionic liquids · liquid crystals · self-assembly

Introduction

Imidazolium-based ionic liquids (IL) have attracted considerable attention as environmentally benign solvents for numerous applications, as in various chemical reactions,[1] for preparation of dye-sensitized solar cells,[2] and light-emitting electrochemical cells,[3] for the stabilization of gold nanoparticles or nanorods,[4] and as ion-conducting materials.[2,5] Liquid crystals (LCs) combining order at the nanometer scale with mobility have found widespread application, for example, in display technology.[6,7] Combining the self-organization forces of liquid crystals with the unique solvent properties and ion-conducting properties of imidazolium ionic liquids yielded imidazolium-based ionic liquid crystals (ILCs).[6,8,9] These LC materials lead to novel applications as, for example, in direction-dependent ion-conducting materials[6] and have improved the light-to-electric energy conversion efficiency of dye-sensitized solar cells.[10,11] Very recently, mesomorphic imidazolium salts were also used as new vectors for small interfering RNA (siRNA) transfection.[12] Hence, for the exploration of further applications the study of the self-assembly behavior and the structure–property relationships of imidazolium-based ILCs is essential.

There are several distinct modes of self-assembly in liquid-crystalline soft matter (see Figure 1). These are the

[a] Prof. Dr. X. Cheng, X. Bai, S. Jing
Key Laboratory of Medicinal Chemistry for Natural Resources
Yunnan University, Kunming, Yunnan 650091 (P.R. China)
Fax: (+86) 871-5032905
E-mail: xhcheng@ynu.edu.cn

[b] Dipl.-Chem. H. Ebert, Dr. M. Prehm, Prof. Dr. C. Tschierske
Institute of Chemistry, Martin-Luther University Halle-Wittenberg
Kurt-Mothes Strasse 2, 06120 Halle/Saale (Germany)
Fax: (+49) 345-55-27346
E-mail: carsten.tschierske@chemie.uni-halle.de

Supporting information for this article is available on the WWW under http://dx.doi.org/10.1002/chem.200903210.

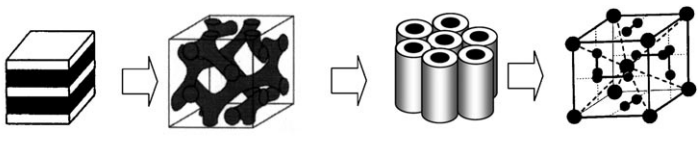

Figure 1. Mesophase morphologies observed in nanosegregated thermotropic LC systems occurring with increasing interface curvature in the self-assembled system and their inherent properties; 1D, 2D, and 3D indicate the dimensionality of the crystallographic lattice; 0-*d*,1-*d*, 2-*d*, and 3-*d* indicate the dimensions of connectivity of the aggregates, as for example expressed by the directionality of conducting properties (3-*d* = conduction in all three directions;1-*d*, 2-*d*, in one and two directions, respectively; 0-*d* = insulator, if the conducting path, shown in black, is inside the aggregates[14,18c]); abbreviations Sm = smectic (lamellar) phase, Cub$_V$ = bicontinuous cubic phase, Col$_{hex}$ = hexagonal columnar phase, and Cub$_I$ = micellar (discontinuous, spheroidic) cubic phase.[16,18,25]

nematic phases, widely used nowadays in LC displays, having only orientational order (not shown in Figure 1), the smectic phases representing lamellar organizations (Sm), the columnar phases formed by cylinders packed on an, in most cases, hexagonal 2D lattice (Col$_{hex}$), and two distinct types of cubic phases (Cub$_V$ and Cub$_I$). In contrast to the nematic, lamellar, and columnar LC phases with direction-dependent properties, such as electron-, hole-, or ion-conducting,[6,13] as well as optical properties, the cubic phases have isotropic, that is, direction-independent properties. There are two distinct types of cubic phases (see Figure 1). The bicontinuous cubic phases (Cub$_V$), appearing as intermediate phases at the transition from lamellar to columnar organization, form different types of continuous interwoven 3D networks of channels. The other type, the so-called micellar cubic phases (Cub$_I$) is based on the complex self-assembly of spheroidic supramolecular aggregates. Hence, inducing a transition between anisotropic mesophases with distinct directionality of conducting properties (Sm = 2-*d*; Col = 1-*d*) and isotropic cubic phases that can be either insulators (Cub$_I$) or isotropic conducting materials (Cub$_V$; provided that the ion-conducting path is inside the aggregates in all cases) is a useful tool for tailoring the application properties of ionic liquid-crystalline materials (Figure 1).[14,15,18c] Though cubic phases are well-known modes of self-assembly in lyotropic systems, in thermotropic LCs these superstructures are relatively rare. In particular, the thermotropic micellar cubic phase was only recently discovered, at first for carbohydrate-based amphiphiles.[16] Although nowadays these mesophases have been found in the phase sequences of several different types of taper-shaped and dendritic amphiphilic molecules[17–24] based on nanosegregation,[25] including the first examples of taper-shaped imidazolium salts (see Scheme 1),[14,26] the

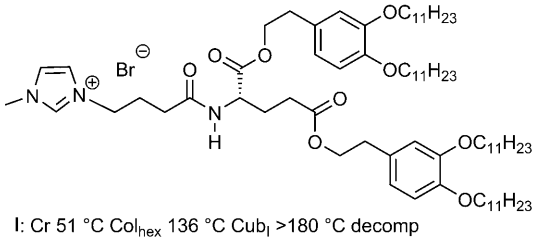

I: Cr 51 °C Col$_{hex}$ 136 °C Cub$_I$ >180 °C decomp

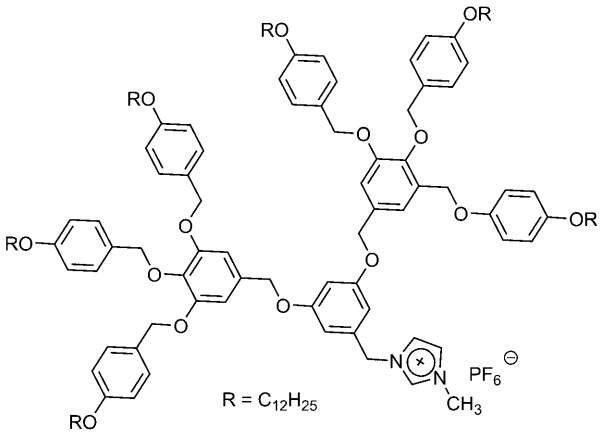

II: Cr 48 °C Col$_{hex}$ 108 °C Cub$_I$ 179 °C Iso

Scheme 1. Previously reported examples of imidazolium salts forming micellar cubic phases.[14,26]

design of materials forming these micellar cubic phases is still a challenge. In particular, for the exploration of further applications of imidazole-based ILCs, the study of the LC self-assembly behavior dependent on the molecular structure of these ILCs is essential.

Presently, there are four classes of imidazole-based ILCs: 1) Imidazolium-based amphiphilic LCs with one or two long

Abstract in Chinese:

通过芳胺化作用合成了一系列基于棒状形的 1-苯基-1H-咪唑液晶(LCs)及基于相应咪唑盐的离子液晶(ILCs). 修饰了 C-端链(位于刚硬棒状核的无电荷一端)及 N-端链(位于咪唑盐环上)的长度和数目, 采用偏光显微镜(POM), 差示扫描量热仪(DSC)及 X 衍射等手段研究了这些结构参数的改变对液晶相中分子组装模式的影响. 在单链的咪唑衍生物中发现了向列相 (N)和双分子层状结构的近晶相(SmA_2); 增加 C-端链的数目, 单链的咪唑衍生物的液晶性质会消失; 但是对于相应的咪唑盐来说, 增加 C-端链的数目, 分子保持了液晶性, 并发生了从近晶相 (SmA) 到六方柱相(Col_{hex}), 再到胶束立方相($Cub_I/Pm\bar{3}n$)的转变; 而增长 N-端链长度, 出现相反的液晶相系列. 在带很短的 N-端链的液晶相中, 分子倾向于采取尾对尾的堆积方式, 导致 N-端链与 C-端链分离; 延长 N-端链, 导致 N-端和 C-端链混合交叉排布, 同时芳香核完全交叠在一起。对于 smectic 相, N-端链长度的增加, 导致了双分子层的近晶相(SmA_2)向单分子层的近晶相(SmA)的转变; 对于柱相和三维立方相, 相互分离的尾对尾的堆积导致核壳结构的形成. 延长 N-端链, 会破坏核壳结构的形成, Cub_I 和 Col 相也就随之消失, 取而代之的是具有单分子层状结构的近晶相的形成 (SmA)。因此, 通过对 N-端链长的修饰, 可使这类分子从锥形液晶元变成多链形液晶元, 从而实现对这类离子液晶自组装行为的有效控制。

alkyl chains,[27–30] in some cases incorporating an additional benzene ring in the lipophilic chain(s),[31] giving predominately thermotropic (in the absence of solvents) and lyotropic (in the presence of solvents) smectic phases. 2) Taper-shaped imidazolium salts with multiple alkyl chains provide predominately columnar phases,[14,15b,c,32–34] but more recently, the first examples of bicontinuous cubic,[12] micellar cubic,[14,26] and 3D tetragonal phases[26] were observed for dendritic imidazolium compounds, such as **I** and **II** (see Scheme 1). The LC properties of these imidazolium salts originate mainly from their strongly amphiphilic character and the space filling of the lipophilic chains. 3) The third type is provided by rodlike[3,15a,35–40] and disclike mesogens,[41–45] which are connected with imidazolium moieties by relatively long flexible spacers. In this case, mesogenity is mainly based on the self-assembly of the anisometric mesogenic unit (smectic for rodlike and columnar for disclike units), which is then modified by the segregation of the imidazolium unit.[15a,42,46] Because of the strong intermolecular electrostatic interactions, smectic and in some cases also columnar phases are stabilized and nematic mesophases are removed for such systems.[9,28,47] 4) Rodlike or slightly bent molecules in which the imidazolium group is an integral part of the rigid core unit either in the center[48–50] or at the periphery[51] represent the fourth and least investigated class of imidazole-based ILCs. Whereas for noncharged 3-substituted 1*H*-imidazole amphiphiles the number of alkyl chains attached to the imidazole-terminated rodlike core was modified and in this way columnar and micellar cubic mesophases based on hydrogen-bonded aggregates were obtained,[52,53] to our knowledge no such investigation has been carried out for charged imidazolium-based rodlike mesogens. Only rodlike molecules (mostly 1-(4′-substituted 1,1′-biphenyl-4-yl)-1*H*-imidazolium salts) with single chains attached to both ends have been recently reported by Kouwer and Swager with respect to the effects of chain length, chain branching, and the nature of the counterion on the mesophase properties.[51] Due to this calamitic (rodlike) molecular structure, smectic phases (mostly SmA phases) were exclusively observed that have either a bilayer or monolayer structure.[51]

Herein we present the first systematic study of the effects of length and number of alkyl chains on the LC properties of phenyl benzoate based rodlike imidazolium salts **1^n/*m*–3^n/*m***[54] and their nonionic precursors, the 1-phenyl-1*H*-imidazoles **1^n/0–3^n/0**.[55] In all the LC imidazolium salts reported herein bromide anions were used as counterions. In the notation of the compounds (see Scheme 2) the compound number indicates the number of alkyloxy chains at the benzoate moiety (C-terminal chains); the superscript *n* indicates the length of these C-terminal chains (even-numbered chains with $n=6$–18); the number *m* (after the slash) identifies the length of the alkyl chain attached to the imidazole moiety (N-terminal chain, $m=0$ for noncharged imidazoles and $m=2$–6, 8, 10, 12, 14, and 18 for the imidazolium salts). In this report the assignment of the compounds to the series of single-, double-, or triple-chain compounds is exclusively based on the number of C-terminal chains, irrespective of whether there is an additional N-terminal chain or not.

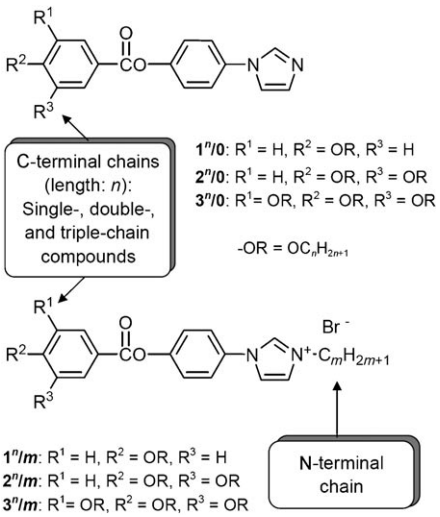

Scheme 2. Imidazole-based nonionic (**1^n/0–3^n/0**) and ionic (**1^n/*m*–3^n/*m***) rodlike, taper-shaped, and polycatenar mesogens under investigation and the notations used for these compounds; the compound numbers **1**–**3** indicate the number of C-terminal chains, *m* indicates the length of the N-terminal chain (0 means the absence of a chain, that is, noncharged imidazole-based mesogens) and the superscript number (*n*) gives the number of C atoms in each of the C-terminal chains. The assignment of the compounds as single-, double-, and triple chain is based on the number of C-terminal chains, irrespective of whether there is an additional N-terminal chain or not.

Only nematic (N) and bilayer smectic phases (SmA_2) were observed for the single-chain nonionic molecules **1^n/0**, and LC phases were lost by increasing the number of C-terminal chains, but in the series of related imidazolium salts a transition from SmA phases via hexagonal columnar phases (Col_{hex}) to micellar cubic phases (Cub_I) with a *Pm*3*n* lattice was observed by increasing the number and the length of the C-terminal chains. These are the first micellar cubic phases formed by imidazolium-based ILCs with extended rodlike aromatic cores. It was also found that the mode of self-assembly in this class of ILC is mainly determined by the length of the N-terminal chain. Very short chains prefer an end-to-end packing of the mesogens in which the N-terminal chains are segregated from the C-terminal chains. Elongation of the N-terminal chain leads to a mixing of N- and C-terminal chains that is accompanied by complete intercalation of the aromatic cores. In the smectic phases this gives rise to a transition from bilayer (SmA_2) to monolayer smectic (SmA) phases. For the columnar and cubic phases the segregated end-to-end packing leads to core–shell aggregates, composed of lipophilic cores that contain the N-terminal chains, which are enclosed by shells of the ionic moieties and the aromatic parts. These core–shell aggregates adopt a long-range order in the lipophilic continuum of the fluid C-terminal chains. Elongation of the N-terminal chains inhibits core–shell formation and removes Cub_I and Col phases in favor of single-layer SmA phases. Effectively, by tailoring the length of the N-terminal chain, a crossover from taper-

shaped to polycatenar LC tectons was achieved that allows the control of ILC self-assembly.

Results and Discussion

Synthesis: The synthesis of the nonionic imidazoles **1^n/0–3^n/0** and the imidazolium salts **1^n/*m*–3^n/*m*** is shown in Scheme 3 (for experimental details, see the Supporting Information).

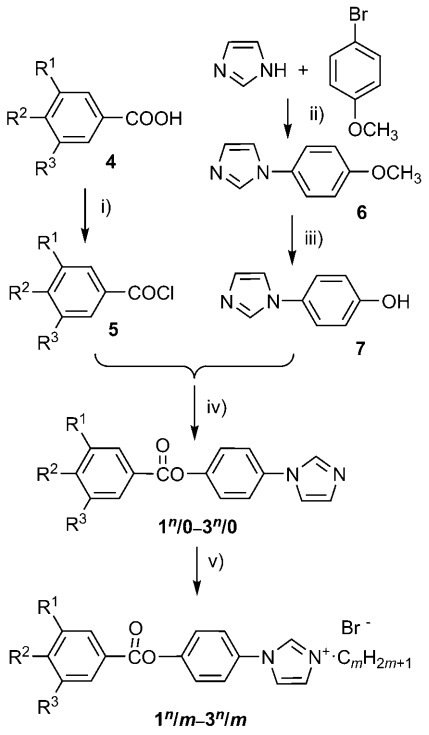

Scheme 3. Synthesis of compounds **1^n/*m*–3^n/*m***. Reagents and conditions: i) $SOCl_2$, reflux, 5 h; ii) K_2CO_3, CuI, *N*-methyl-2-pyrrolidone, 24 h, 150 °C; iii) 48 % HBr, 18 h, 130 °C; iv) NEt_3, THF, RT, 48 h; v) 1-bromoalkane, toluene, reflux, 18 h.

The key step in the synthesis was an Ullman-type coupling[56] of 4-bromoanisole with imidazole, which gave 1-(4-methoxyphenyl)-1*H*-imidazole (**6**).[51] Demethylation of **6** using 48 % HBr[57] yielded 4-(1*H*-imidazol-1-yl)phenol (**7**), which was acylated with the appropriate benzoyl chloride (**5**), leading to the 1-(4-benzoyloxyphenyl)-1*H*-imidazoles **1^n/0–3^n/0**. These compounds were quaternized with appropriate *n*-alkyl bromides to yield the imidazolium-based ILCs **1^n/*m*–3^n/*m***. Purification of the products was done by crystallization from methanol/chloroform (10:1) or by column chromatography; the structure and purity of all compounds were confirmed by ^{1}H NMR spectroscopy and elemental analysis (see Tables S3–S6 in the Supporting Information).

Investigations: The liquid-crystalline properties of the nonionic imidazoles **1^n/0–3^n/0** and the corresponding imidazolium compounds **1^n/*m*–3^n/*m*** were studied by polarizing optical microscopy (POM, Optiphot 2, Nikon, in conjunction with a FP 82 HT heating stage, Mettler), differential scanning calorimetry (DSC, DSC-7, Perkin–Elmer), and for selected compounds, by X-ray diffraction (XRD) using surface-aligned samples on a glass plate by means of a 2D detector (HI-STAR, Siemens, beam direction parallel to the surface). Single crystals of compounds **1^{10}/0** and **1^{12}/0** were obtained by slow crystallization from $CHCl_3$ and these were used for crystal-structure determination on a diffractometer with a CCD area detector (Smart Apex II, Bruker, $Mo_{K\alpha}$, $\lambda =$ 0.71073 Å). The complete conditions of the data collection and structure refinement are given in Figures S23–S27 in the Supporting Information.

Liquid-crystalline properties of the nonionic imidazole derivatives: The transition temperatures of the nonionic imidazoles **1^n/0–3^n/0** are collected in Table 1. Single-chain compounds **1^n/0** exhibit thermotropic nematic phases for short-chain compounds and smectic A phases for compounds with longer chains, while double- and triple-chain derivatives **2^n/0** and **3^n/0** are only crystalline materials without LC phases. Under POM, the nematic phases are characterized by their typical marble or schlieren textures (Figure S1a in the Supporting Information). The SmA phases were identified by textures consisting of focal conics, fanlike textures, and pseudoisotropic regions with oily streaks, depending on the alignment conditions (Figure S1b in the Supporting Information). The pseudoisotropic regions indicate an on average orthogonal organization of the molecules with respect to the layer planes.[58] The SmA phases of compounds **1^{10}/0** and

Table 1. Mesophases, transition temperatures (T in °C), and transition enthalpy values (ΔH in kJ mol^{-1}) of the 4-(1*H*-imidazol-1-yl-phenyl) benzoates **1^n/0–3^n/0**.[a]

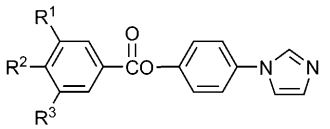

	R^1	R^2	R^3	Phase and T[ΔH]
1^6/0	H	OC_6H_{13}	H	Cr 120[33.6] (N 100[0.4]) Iso
1^7/0	H	OC_7H_{15}	H	Cr 107 SmA_2 110 N 125 Iso[b]
1^8/0	H	OC_8H_{17}	H	Cr 105 SmA_2 126 Iso[b]
1^{10}/0	H	$OC_{10}H_{21}$	H	Cr 100[26.7] SmA_2 125[2.9] Iso
1^{12}/0	H	$OC_{12}H_{25}$	H	Cr 97[32.7] SmA_2 127[3.8] Iso[c]
1^{18}/0	H	$OC_{18}H_{37}$	H	Cr 99[75.6] SmA_2 132[5.6] Iso
2^{12}/0	$OC_{12}H_{25}$	$OC_{12}H_{25}$	H	Cr 119 Iso[b]
2^{16}/0	$OC_{16}H_{33}$	$OC_{16}H_{33}$	H	Cr_1 89[37.2] $Cr_2$104[29.6] Iso
3^{12}/0	$OC_{12}H_{25}$	$OC_{12}H_{25}$	$OC_{12}H_{25}$	Cr 63 Iso[b]
3^{14}/0	$OC_{14}H_{29}$	$OC_{14}H_{29}$	$OC_{14}H_{29}$	Cr 87 Iso[b]
3^{16}/0	$OC_{16}H_{33}$	$OC_{16}H_{33}$	$OC_{16}H_{33}$	Cr 79[107] Iso

[a] Transition temperatures and enthalpy changes (in square brackets) were determined by DSC (peak temperature, first heating scan, 10 K min^{-1}), values in parentheses indicate monotropic (metastable) phases. Abbreviations: Cr = crystalline solid, N = nematic phase, SmA_2 = smectic A phase with intercalated bilayer structure,[60] Iso = isotropic liquid state; for more details see Figures S1–S5 in the Supporting Information. [b] Transition temperatures were determined by POM. [c] See ref. [51].

1^{12}/0 were additionally confirmed by X-ray investigation of the aligned samples (Figure 2 and Figures S2–S5 in the Supporting Information). The diffraction pattern of **1^{10}/0**, for example, shows strong sharp fundamental layer reflections on

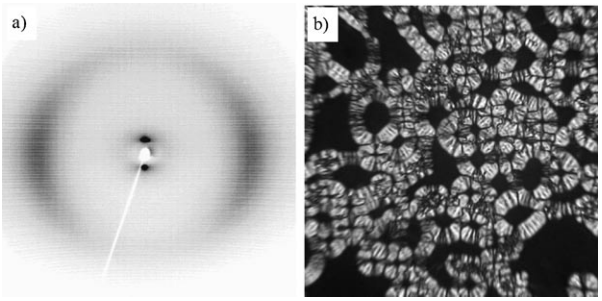

Figure 2. a) X-ray diffraction pattern of an aligned sample of the SmA phase of compound **1^{10}/0** at $T=110\,°C$; b) oily streaks texture of compound **1^{12}/0** (crossed polarizers) at 105 °C (dark areas represent homeotropically aligned regions).

the meridian along with diffuse outer scatterings with maxima of the intensity on the equator. This confirms a layer structure in which the long axes of the molecules are on average perpendicular to the layers. The maxima of the outer diffuse scatterings at $d=0.45$ nm correspond to the average lateral distances between the molecules in the fluid LC state. The layer spacings in the SmA phases of compounds **1^{10}/0** and **1^{12}/0** are $d=3.4$ and 3.7 nm, respectively. Compared with the molecular lengths in the most stretched conformations ($L=2.9$ nm and 3.2 nm, respectively[59]), the layer thickness is larger than the molecular length ($d/L=$ 1.2, see Table 2), but significantly smaller than twice the length, indicating bilayer structures with complete intercalation of the alkyl chains (SmA_2) as shown in Figure 3a.[60]

Table 2. Comparison of X-ray data and molecular dimensions of the SmA phases of imidazoles **1^n/0** and the single-, double-, and triple-chain imidazolium bromides **1^n/*m*–3^n/*m***.[a]

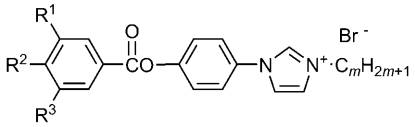

	R^1	R^2	R^3	*m*	*d* [nm] (*T* [°C])	*L* [nm]	*d*/*L*
1^{10}/0	H	$OC_{10}H_{21}$	H	–	3.4 (110)	2.9	1.2
1^{12}/0	H	$OC_{12}H_{25}$	H	–	3.7 (120)	3.2	1.2
1^{12}/3	H	$OC_{12}H_{25}$	H	3	5.4 (150)	3.6	1.5
1^{12}/4	H	$OC_{12}H_{25}$	H	4	4.1 (170)	3.7	1.1
1^{12}/12	H	$OC_{12}H_{25}$	H	12	3.7 (175)	4.7	0.8
1^{12}/18	H	$OC_{12}H_{25}$	H	18	4.1 (170)	5.5	0.8
2^{12}/4	$OC_{12}H_{25}$	$OC_{12}H_{25}$	H	4	4.4 (100)	3.7	1.2
2^{12}/12	$OC_{12}H_{25}$	$OC_{12}H_{25}$	H	12	3.6 (160)	4.7	0.8
3^{12}/8	$OC_{12}H_{25}$	$OC_{12}H_{25}$	$OC_{12}H_{25}$	8	3.8 (70)	4.2	0.9

[a] Abbreviations: d = layer spacing; L = molecular length measured between the ends of the terminal chains and assuming a most stretched conformation with all-*trans* conformation of the alkyl chains.[59] For more details see Figures S2–S12, S16 and Table S1 in the Supporting Information.

Single-crystal structures of the crystalline phases were obtained for compounds **1^{10}/0** and **1^{12}/0**. For both compounds, a triclinic symmetry was observed with space group $P\bar{1}$ with two molecules per unit cell.[61] Typical motifs of the organi-

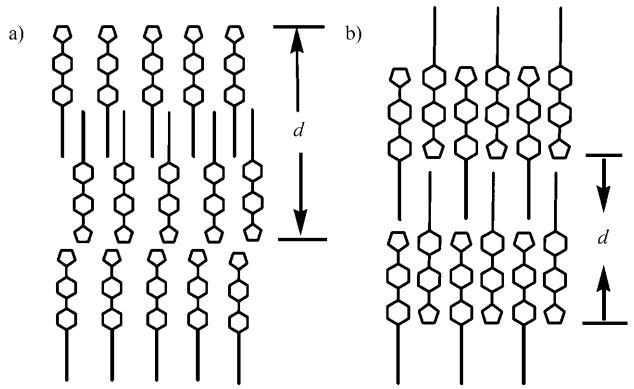

Figure 3. Models of two possible structures of SmA phases of compounds **1^n/0**: a) bilayer structure with parallel organization of the aromatic cores inside the layers and antiparallel organization of the layers with intercalated C-terminal chains (SmA_2)[60] as observed for compounds **1^n/0**; b) monolayer SmA structure with antiparallel organization of the rodlike cores inside the layers; this arrangement is only observed if sufficiently long alkyl chains are attached to the N-terminal ends of the molecules.

zation of the molecules in these crystal structures (see Figure 4 and Figures S23–S27 in the Supporting Information) are staggered end-to-end pairs of the aromatic cores, which are arranged side-by-side in an antiparallel fashion in

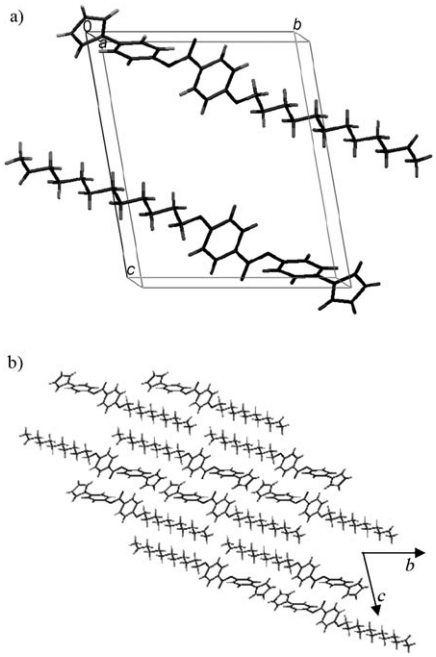

Figure 4. a) Unit cell of the single-crystal structure of **1^{12}/0**; b) crystal packing on the (*bc*) plane; for other details and the crystal structure of **1^{10}/0**, see Figure S23–S27 in Supporting Information.

ribbons (Figure 4b) leading to an overall structure that can be regarded as a broken lamellar structure with strongly tilted molecules (Figure 4b). The end-to-end organization is also observed for the liquid-crystalline SmA_2 phases of compounds **1^{10}/0** and **1^{12}/0**, but in contrast to the crystal structures, in the LC phases there is a nontilted and parallel side-by-side packing of the molecules inside the layers, leading to the bilayer structure with intercallated alkyl chains (see Figure 3a). This difference between crystal and LC structure might be due to the different properties of the alkyl chains in these two states of matter. In the crystalline state the alkyl chains are rigid and pack parallel to the aromatic rods, leading to ribbons of antiparallel aromatics separated by ribbons of antiparallel alkyl chains to optimize space filling and maximize attractive intermolecular interactions. In the LC state the alkyl chains are molten and these flexible chains become incompatible with the still rigid aromatics (rigid–flexible incompatibility), which induces the segregation of these chains into infinite layers to minimize the aromatic–aliphatic interfaces. The antiparallel end-to-end packing is retained, but the side-to-side packing becomes parallel to allow complete segregation of the flexible alkyl chains and the rigid aromatics (see Figure 3a). As will be shown later, if an N-terminal alkyl chain of sufficient length is introduced, the antiparallel side-by-side packing can be restored, leading to monolayer smectic phases as sketched in Figure 3b. Hence, the crystal structures contribute to the understanding of the observed structural transitions in the LC phases.

In summary, for the single-chain compounds **1^n/0**, upon elongation of the terminal alkoxy chain, the mesophase type changes from nematic to bilayer SmA_2, accompanied by almost constant melting points and a slight increase of the clearing points, giving rise to slightly increasing mesophase ranges due to the increase of van der Waals interactions and nanosegregation upon increasing the alkyl chain length. Mesophases were lost if the number of chains was increased; all synthesized compounds **2^n/0** and **3^n/0** with two or three alkyl chains show only crystalline phases (see Table 1).

Liquid-crystalline properties of the ionic imidazolium salts: In contrast to the series of noncharged imidazoles **1^n/0–3^n/0**, in the series of the imidazolium salts **1^n/*m*–3^n/*m*** most compounds show LC phases and the variety of different phase types is much broader, including monolayer and bilayer smectic phases as well as columnar and cubic phases. Due to the additional attractive electrostatic interactions provided by the charged polar groups and also due to the stronger segregation of these groups from the lipophilic molecular parts (polar–apolar incompatibility) the transition temperatures of these compounds, especially those with only one C-terminal chain, are very high. Due to this mesophase stabilizing effect most of the compounds with two or more C-terminal chains also form stable LC phases. The transition temperatures of the synthesized imidazolium bromides are collated in Tables 3, 4, and 5.

Table 3. Mesophases, transition temperatures (T in °C), and transition enthalpy values (ΔH in kJ mol^{-1}) of the single-chain imidazolium bromides **1^n/*m***.[a]

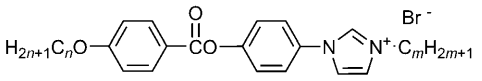

	n	m	Phases and T[ΔH]
1^6/12	6	12	Cr 166[17.6] SmA >200 Iso (decomp)
1^6/18	6	18	Cr 172[23.1] SmA >200 Iso (decomp)
1^8/4	8	4	Cr 199 Iso[b]
1^8/12	8	12	Cr 190 SmA >200 Iso (decomp)[b]
1^{10}/4	10	4	Cr 162[20.4] (SmA_2 154.5 N 155[0.3][c]) Iso
1^{12}/3	12	3	Cr_1 103[22.0] SmA_2 >200 Iso (decomp)[d]
1^{12}/4	12	4	Cr_1 89[5.4] Cr_2 151[15.1] SmA_2 196 Iso (decomp)
1^{12}/12	12	12	Cr 169[23.5] SmA >200 Iso (decomp)
1^{12}/18	12	18	Cr 112[12.6] Cr 149[12.6] SmA >200 Iso (decomp)
1^{18}/6	18	6	Cr 165[22.4] SmA >200 Iso (decomp)
1^{18}/12	18	12	Cr 167 SmA >200 Iso (decomp)[b]

[a] Transition temperature and enthalpy changes (in square brackets) were determined by DSC (peak temperature, first heating scan, 10 K min^{-1}; no transition enthalpies are given for clearing temperatures associated with decomposition). Abbreviations: SmA = SmA phase with monolayer structure, for the other abbreviations, see Table 1. [b] Transition temperatures were determined by POM. [c] Transitions not resolved. [d] At 85 °C, formation of a birefringent Schlieren texture is observed in the homeotropically aligned regions of the SmA phase, most likely indicating a transition to a SmC phase.

*Imidazolium bromides with one C-terminal chain **1^n/m***: The transition temperatures of the single-chain imidazolium bromides **1^n/*m*** are collated in Table 3. These compounds have two flexible chains, one at each end of the rodlike aromatic core, and hence, these compounds can be regarded as rodlike ILCs. Compound **1^8/4**, which has a total of 12 carbon atoms in the hydrocarbon chain, is a high-melting crystalline solid. All the other single-chain compounds with a total number of more than 12 carbon atoms in their chains form SmA phases with focal conic textures and homeotropic areas separated by oily streaks (see Figure 2b). Only compound **1^{10}/4**, the shortest homologue with LC properties, has a very small range of a nematic phase above the SmA phase. With the exception of this compound all the other compounds have exclusively SmA phases with high clearing temperatures, in most cases above 200 °C. The clearing temperatures for most of these compounds cannot be determined precisely, due to significant decomposition at these high temperatures. The SmA-to-Iso transition temperatures seems at first to decrease with increasing length of the N-terminal chain from **1^{12}/3** to **1^{12}/4** and then, after going through an apparent minimum, increase again to >200 °C for compounds **1^{12}/12–1^{12}/18** with long N-terminal chains (see Table 3).

The XRD patterns of the smectic phases are similar to those observed for the noncharged imidazoles, characterized by the fundamental layer reflection, in some cases associated with the second-order layer reflection, and a diffuse wide-angle scattering (see Figures S6–S9 in the Supporting Information). Unexpectedly, the layer spacing d strongly decreases with elongation of the N-terminal chain from d =

5.4 nm for $m=3$ to $d=3.7$ nm for $m=12$ and then slightly increases again to $d=4.1$ nm for $m=18$ (see Table 2). The layer spacing of compounds **1[12]/3** and **1[12]/4** with short N-terminal chains is larger than the molecular length ($d/L=1.5$ and 1.1, respectively) but significantly smaller than twice the length, which indicates a bilayer structure with significant intercalation of the alkyl chains (SmA_2, see Figure 5a), similar

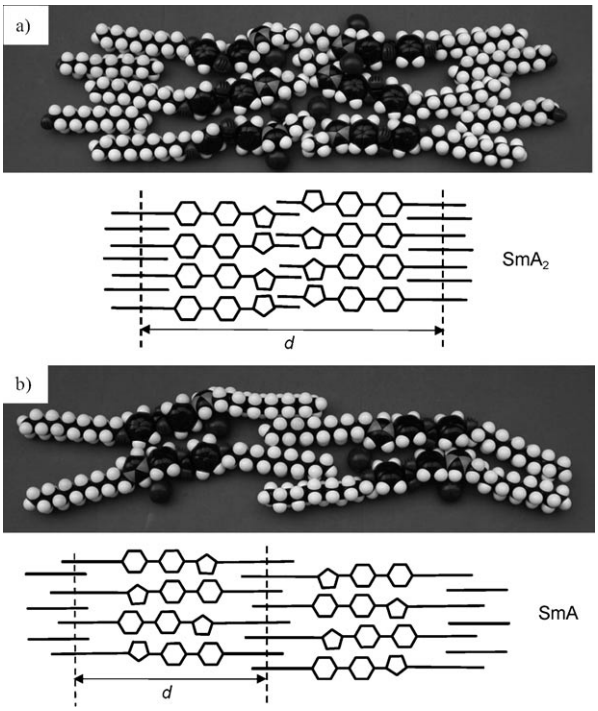

Figure 5. CPK models[59] and schematic sketches showing a) the organization of **1[12]/3** in a double-layer SmA_2 phase and b) the organization of compound **1[12]/12** in a monolayer SmA phase.

to the SmA_2 phases of the imidazoles **1[n]/0**, shown in Figure 3a.[60] The d/L ratio decreases with increasing length of the N-terminal chain from **1[12]/3** to **1[12]/4** and for compound **1[12]/12** with a long N-terminal chain the layer spacing is smaller than the molecular length[59] ($d/L=0.8$), which indicates a monolayer structure as shown in Figure 5b. Further increase of the length of the N-terminal chain (compound **1[12]/18**) does not change the d/L ratio significantly. It is proposed that in the bilayer SmA_2 phases of the imidazolium salts with short N-terminal chains the charged imidazolium groups are separated by a thin lipophilic layer formed by the N-terminal chains (see Figure 5a). Elongation of the chains increases the thickness of these lipophilic layers, which reduces the stability of the bilayer smectic phase, probably due to the creation of high-energy interfaces between the highly polar surfaces of the imidazolium sides of the aromatic sublayers and the nonpolar layers formed by the N-terminal chains. The bilayer SmA_2 phase is replaced by a monolayer structure if the N-terminal chain becomes sufficiently long to accommodate the C-terminal chains, giving rise to a mixing of N- and C-terminal chains. In the resulting monolayer structure the parallel side-by-side packing of the aromatic units inside the layers is removed, which seems to be favorable as it maximizes entropy and allows direct dipole compensation between adjacent molecules inside the layers (see Figure 5b). Moreover, in the monolayer structure the same antiparallel side-by-side packing of the aromatics, as observed in the crystal structures of compounds **1[10]/0** and **1[12]/0** (see Figure 4) is achieved. Hence, it seems that monolayer formation is favored as soon as compatibility of the lengths of the N-terminal and the C-terminal chains is achieved and this gives rise to extremely stable smectic phases with high transition temperatures. The difference between L and d in the single-layer structure might be a consequence of a relatively low order parameter of the aromatics, which is reduced due to the presence of the distortion caused by the bulky bromide counterions, by chain folding and by intercalation of the alkyl chains to achieve optimal space filling (see Figure 5b).

Imidazolium bromides with two C-terminal chains ***2[n]/m***: In the series of compounds **2[n]/m** with two C-terminal alkyloxy chains (see Table 4) SmA phases were exclusively found as

Table 4. Mesophases, transition temperatures (T in °C), and transition enthalpy values (ΔH in kJ mol^{-1}) of the double-chain imidazolium bromides **2[n]/m**.[a]

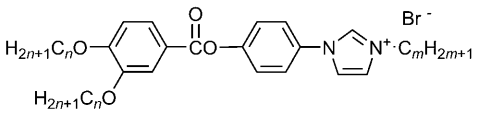

	n	m	Phases and T[ΔH]
2[12]/4	12	4	Cr 51[24.8] SmA_2 >225 Iso (decomp)
2[12]/8	12	8	Cr 62 SmA 223 Iso[b]
2[12]/12	12	12	Cr_1 95[23.8] Cr_2 106[14.4] SmA 186[1.5] Iso
2[16]/4	16	4	Cr 74[40.4] SmA_2 170[0.1] Iso

[a] Transition temperature and enthalpy changes (in square brackets) were determined by DSC (peak temperature, first heating scan, 10 K min^{-1}). For abbreviations see Table 1. [b] Transition temperatures were determined by POM.

confirmed by the typical textural features as well as by X-ray diffraction (see Figure 6 and Figures S10–S12 in the Supporting Information). The SmA-to-Iso transition temperatures are lower than those of related single-chain compounds **1[n]/m** and these temperatures decrease upon elongation of either the C-terminal or the N-terminal chain(s), thus indicating a distortion of layer formation by chain elongation, which is opposite to the trends seen for the single-chain compounds **1[n]/m**. This indicates that the increasing space required by the additional chains distorts the packing in the layers. Nevertheless, a similar dependence of the d spacing on the length of the N-terminal chain as reported for the single-chain compounds **1[n]/m** was also observed in the series of double chain compounds **2[n]/m**, that is, compound **2[12]/4** forms an intercalated double layer SmA_2 phase, whereas the SmA phase of compound **2[12]/12** with a longer N-terminal chain is a single-layer SmA phase (see Table 2).

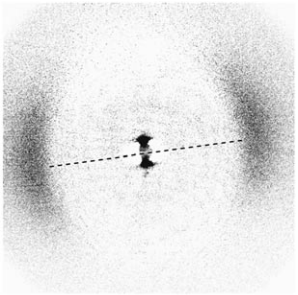

Figure 6. X-ray diffraction pattern of an aligned sample of the SmA phase of compound **2^{12}/4** at $T=100\,°C$ (after subtraction of the diffraction pattern of the isotropic phase; the layer reflections are perpendicular to the equator as indicated by the dashed line; shading gives rise to a lower intensity of the diffuse wide-angle scattering in the lower part).

The reasons for this structural change upon elongation of the N-terminal chain should be essentially the same as discussed for the single-chain compounds in the previous section.

*Imidazolium bromides with three C-terminal chains **3^n/m***

Smectic phases: A series of different LC phases was observed for compounds **3^n/m** with three C-terminal chains (Table 5). SmA phases (confirmed by typical textures using POM) are formed by compounds **3^{12}/8**, **3^{14}/14**, and **3^{16}/5**–**3^{16}/8** with a length of the N-terminal chain of $m>4$. The stability of these SmA phases is much lower than those of the related single-chain and double-chain imidazolium salts and this is in line with the layer distortion that grows with increasing number of chains. This is, for example, seen in the development of the SmA–Iso transition temperatures as observed with growing chain number in the series **1^{12}/12** (>200 °C)–**2^{12}/12** (186 °C)–**3^{12}/14** (no SmA phase).

The stability of the SmA phase also decreases with increasing length of the N-terminal chain (compare, for example, compounds **3^{16}/5**–**3^{16}/8** in Table 5) and it slightly increases with increasing length of the C-terminal chains (compare **3^{12}/8** and **3^{16}/8**). The XRD pattern of **3^{12}/8** (Figure S16 in the Supporting Information) provides a layer distance of $d=$ 3.8 nm that corresponds to a monolayer organization with only weak intercalation of the alkyl chains ($d/L=0.9$). Beside the SmA phases in the series of compounds **3^n/m** there are also columnar and cubic phases that can only be found for molecules with shorter N-terminal chains.

Table 5. Mesophases, transition temperatures (T in °C), and transition enthalpy values (ΔH in kJ mol^{-1}) of the triple-chain imidazolium bromides **3^n/m**.[a]

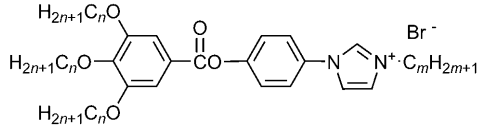

	n	m	Phases and T[ΔH]
3^{12}/3	12	3	Cr_1 92[49.9] Col >200 Iso (decomp)
3^{12}/4	12	4	Cr 111[72.2] Col_{hex} 124[0.5] Iso
3^{12}/8	12	8	Cr 53[61.1] SmA 76[0.3] Iso
3^{12}/14	12	14	Cr_1 47[26.0] Cr_2 65[57.8] Iso
3^{14}/2	14	2	Cr 102[62.5] Cub_I/*Pm3n* 225 Iso (decomp)
3^{14}/3	14	3	Cr 95[65.8] Col 178[1.9] Iso/Iso 160 Cub_I <20 Cr[b,c,d]
3^{14}/4	14	4	Cr 93[58.5] Col_{hex} 120 Iso[b,c]
3^{14}/14	14	14	Cr 78[58.8] (SmA 52[0.6]) Iso
3^{16}/2	16	2	Cr 98[38.3] Cub_I/P*m3n* 225 Iso (decomp)
3^{16}/3	16	3	Cr 106[77.0] Cub_I/P*m3n* 202[0.3] Iso
3^{16}/4	16	4	Cr 109[99.2] Col_{hex} 171[0.4] Iso
3^{16}/5	16	5	Cr 102 SmA 118 Iso[b]
3^{16}/6	16	6	Cr 82[100.8] SmA 99[0.3] Iso
3^{16}/8	16	8	Cr_1 51[18.0] $Cr_2$57[30.8] SmA 96[0.3] Iso

[a] Transition temperature and enthalpy changes (in square brackets) were determined by DSC (peak temperature, first heating scan, 10 K min^{-1}). Abbreviations: Col = columnar phase, most probably Col_{hex}; Col_{hex} = hexagonal columnar phase; Cub_I = cubic mesophase, most probably Cub_I/*Pm3n*; Cub_I/*Pm3n* = micellar cubic mesophase with space group *Pm3n*; for other abbreviations, see Table 1. [b] Transition temperatures were determined by POM. [c] No peak could be found for this transition in the DSC traces. [d] Phase transitions observed on cooling.

Columnar phases: Columnar phases were found for compounds **3^{12}/3**, **3^{12}/4**, **3^{14}/4**, and **3^{16}/4**, that is, for all compounds with short N-terminal alkyl chains with $m=4$ and in the series **3^{12}/m**, also for $m=3$. Elongation of the N-terminal chain leads to a dramatic reduction of the stability of the columnar phases as seen by comparison of compounds **3^{12}/3** and **3^{12}/4**, in which the Col-to-Iso transition is reduced by more than 76 K (Table 5). The textures of these mesophases, as observed by POM, are characterized by typical spherulitic domains as shown in Figure 7a–c for the columnar phase of compounds **3^{12}/4**, **3^{14}/4**, and **3^{16}/4** as examples.[62] The columnar phases of these three compounds were also investigated by XRD (see Figure 7d,e, and Figures S14, S15, S18, S21, and S22 and Table S1 in the Supporting Information). Besides the diffuse wide-angle scattering three small-angle reflections with a ratio of their reciprocal spacings $1:3^{1/2}:2$ were typically observed,[63] which can be indexed to the 10, 11, and 20 reflections of a hexagonal lattice (see, for example, Figure 7d). The 2D X-ray diffraction pattern of a surface-aligned sample of compound **3^{12}/4** is shown as an example in Figure 7e, confirming the hexagonal lattice (Col_{hex}/*p6mm*). The hexagonal lattice parameters (see Table 6) are around 5 nm for all of the investigated compounds. Although XRD was not carried out on all of the columnar phases, based on textural similarities, it is very likely that also the other columnar phases (indicated as Col in Table 5) represent hexagonal columnar phases. The number of molecules organized in a slice of the columns with a height of $h=0.45$ nm (maximum of the diffuse wide-angle scattering), estimated using Equation (1) and assuming a density of $\rho=1\,g\,cm^{-3}$, is between $n=5$ and $n=6$ for the investigated compounds (N_A = Avogadro constant, M = molecular mass; see Tables 6 and Table S2 in the Supporting Information). There is a slight decrease of this number with increasing chain length, which is usually observed and that is due to the increase of the taper angle with the increasing space requirement of the C-terminal chains.[18,21]

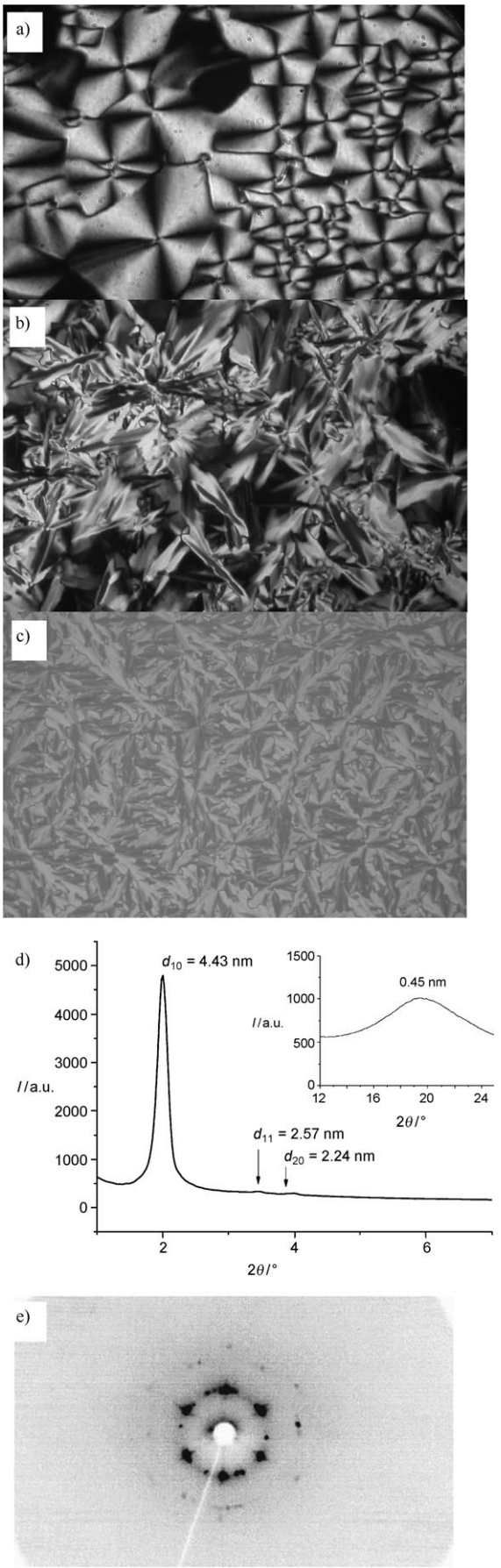

Figure 7. Col_{hex} phases of the imidazolium bromides with three C-terminal chains: Selected texture (crossed polarizers) of compound: a) **3^{12}/4** at 100 °C, b) **3^{14}/4** at 100 °C, c) **3^{16}/4** at 136 °C; d) XRD pattern of **3^{14}/4** (small-angle region, inset shows wide-angle region) at $T = 110$ °C; e) X-ray diffraction pattern of an aligned sample of compound **3^{12}/4** at $T = 110$ °C (multidomain sample); for a color version of the textures, see Figure S13 in the Supporting Information.

Table 6. Comparison of X-ray data and molecular dimensions of the columnar and cubic phases of imidazolium bromides with three C-terminal chains.[a]

	n	m		a [nm] (T [°C])	L [nm]	n
3^{12}/4	12	4	$Col_{hex}/p6mm$	4.9 (110)	3.6	6.0
3^{14}/4	14	4	$Col_{hex}/p6mm$	5.1 (100)	4.0	5.9
3^{16}/4	16	4	$Col_{hex}/p6mm$	5.0 (150)	4.2	5.1
3^{14}/2	14	2	$Cub_I/Pm3n$	10.4 (150)	3.7	85
3^{16}/2	16	2	$Cub_I/Pm3n$	10.8 (150)	4.0	87
3^{16}/3	16	3	$Cub_I/Pm3n$	10.8 (130)	4.1	84

[a] Abbreviations: a = lattice parameter determined by XRD (a_{hex} and a_{cub}, respectively); L = molecular length of a molecule measured between the ends of the terminal chains and assuming a most stretched conformation with all-*trans* conformation of the alkyl chains;[59] n = number of molecules in the cross section of a column in the Col_{hex} phases (with assumed height of 0.45 nm)/respective number of molecules in each micelle of the cubic *Pm3n* lattice ($n_{cell}/8$); for more details see Table 7, and Figures S14, S15, S17–S22 and Tables S1, S2 in the Supporting Information.

$$n = (a^2/2)\sqrt{3}h(N_A/M)\rho \quad (1)$$

There are two distinct modes of self-assembly of taper-shaped molecules; a rosettelike organization and an antiparallel arrangement in ribbons (Figure 8a, b). A rosettelike organization of the molecules (Figure 8a) leads to cylinders with a circular cross section, which gives rise to columnar LC phases with a hexagonal lattice (Col_{hex}).[17,18b] In this arrangement the N-terminal alkyl chains of compounds **3^n/*m***** form a lipophilic core in the middle of the columns, which is surrounded by a polar stratum of the ionic and aromatic parts. These core–shell cylinders are assembled on a hexagonal lattice in the lipophilic continuum of the C-terminal alkyl chains (see Figure 8d). This kind of organization allows a complete segregation of the incompatible units (polar/nonpolar groups as well as short/long alkyl chains), each in its own domain and it requires an interdigitation of the lipophilic C-terminal chains of adjacent columns to fill the space remaining at the periphery (Figure 8e). The effective diameters of the columns (considering this interdigitation) correspond to the experimentally observed hexagonal lattice parameters a_{hex}. This end-to-end organization of the molecules with strong interdigitation of the C-terminal alkyl chains is related to the SmA_2 double-layer structure observed for the smectic phases of the single- and double-chain compounds with short N-terminal chains (see Figures 3a and 5a). However, in this columnar arrangement the space available for the packing of the N-terminal chain inside the column cores is strongly limited and enlarging these chains strongly disfavors this type of organization. This is thought to be the reason for the strong decrease of the stability of the Col phases upon slight elongation of the

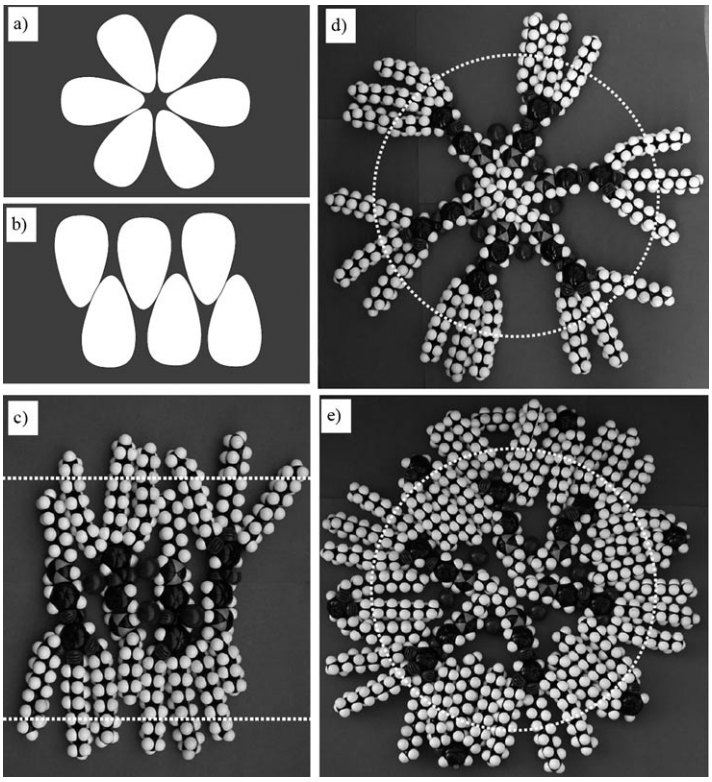

Figure 8. Models showing the organizations of the triple-chain molecules in the LC phases: a) schematic sketches of a rosette, forming cylinders with a circular cross section; b) an antiparallel organization of the molecules leading to ribbonlike aggregates; CPK molecular models showing the organization of the molecules c) in the SmA phase of compound **3^{12}/8** with complete intercalation of the aromatic cores; d,e) in the Col_{hex} phase of compound **3^{12}/3**. (d) shows the cross section through a single column, composed of a lipophilic core containing the N-terminal chains in the middle, the polar shell mainly formed by the bromide ions and the imidazolium units, and the lipophilic shell of the C-terminal alkyl chains around it; it is clear that a dense packing in the periphery cannot be achieved in this arrangement and this requires the intercalation with the chains of adjacent columns. (e) shows the same column with the alkyl chains of adjacent columns filling the space in the lipophilic periphery by intercalation; the regions inside the dotted circles/lines show the dimensions provided by the experimentally observed d values ($d=3.8$ nm) and hexagonal lattice parameters ($a_{hex}=4.9$ nm), respectively; the organization in the cross section of the spheroidic aggregates forming the Cub_I phases is related to those shown in (d) and (e).

N-terminal chains by only one CH_2 group (**3^{12}/3** vs. **3^{12}/4**, see Table 5).

Elongation of the N-terminal chains also enhances the influence of the rodlike shape of the aromatic core on the self-assembly of compounds ***3^n/m***, as it favors an antiparallel packing of the molecules. This antiparallel packing is favorable for the compensation of dipole moments and it reduces the excluded volume between the rods. The complete interdigitation of the aromatic parts reduces the aromatic–lipophilic interface curvature and integrates the N-terminal alkyl chains into the lipophilic regions formed by the C-terminal chains (see Figure 8c). These two effects lead to a transition from a rosettelike organization in the Col_{hex} phases to a ribbonlike antiparallel organization as shown in Figure 8b, more favorable for formation of SmA phases with flat interfaces. The layer distance measured for the SmA phase of compound **3^{12}/8** ($d=3.8$ nm) is in full agreement with this model (Figure 8c). This organization in the SmA phases is fundamentally the same as in the single-layer SmA phases observed for the single- and double-chain compounds with long N-terminal alkyl chains. These SmA phases are destabilized upon elongation of the N-terminal chains (compare compounds **3^{16}/5**–**3^{16}/8** in Table 5), as the lipophilic regions expand, which is unfavorable for the dense packing of the aromatic cores. In contrast, the mesophase stability of the SmA phases of single-chain compounds increases upon chain elongation (see Tables 1 and 3), probably because in this case the packing density of the alkyl chains is improved. In some respects, the change of the molecular structure achieved by elongation of the N-terminal chain provides an example of a change of the mode of self-assembly upon transition from a taper-shaped to a polycatenar molecular structure of the mesogens.

Cubic phases: For the triple-chain imidazolium bromides ***3^n/m*** with very short N-terminal chains ($m=2$, 3) and three relatively long C-terminal chains ($n=14$, 16) optically isotropic mesophases were observed, which are not fluid, but soft and viscoelastic. By increasing the temperature, sharp transitions to highly fluid isotropic liquids occur at defined temperatures, which can also be detected as distinct peaks in the DSC traces (Figure 9). The formation of the isotropic mesophases can be supercooled as typical for mesophases with 3D periodicity (see inset in Figure 9). These POM and DSC observations are indicative of cubic mesophases.[64]

The isotropic mesophases of compounds **3^{14}/2**, **3^{16}/2**, and **3^{16}/3** were investigated by XRD. The diffraction patterns are characterized by a diffuse scattering in the wide-angle region, indicating the fluid LC state, and several reflections in the small-angle region that could be indexed to a cubic lattice with *Pm3n* space group (see Table 7, and Table S1 and Figures S17, S19, and S20 in the Supporting Information). The *Pm3n* lattice is the most commonly observed lat-

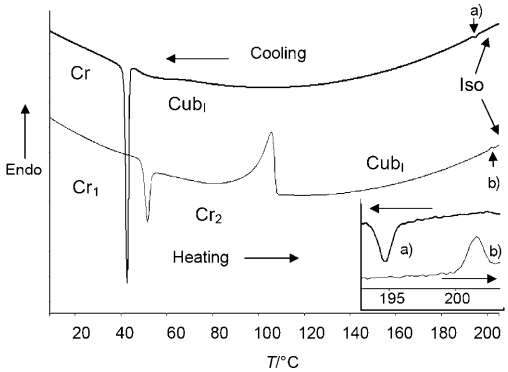

Figure 9. DSC heating and cooling curves of compound **3^{16}/3** (10 K min^{-1}); the inset shows an enlargement of the DSC peaks corresponding to the Iso–Cub and Cub–Iso transition a and b, respectively, indicating a significant supercooling of this phase transition.

Table 7. Crystallographic data of the *Pm3n* cubic phase of compound **3^{16}/3** at $T=170\,^{\circ}C$.[a]

$2\theta_{obsd}$ [°]	d_{obsd} [nm]	*hkl*	d_{calcd} [nm]	$d_{obsd}-d_{calcd}$
1.615	5.47	200 ($\sqrt{4}$)	5.38	0.09
1.837	4.81	210 ($\sqrt{5}$)	4.81	0.00
2.015	4.38	220 ($\sqrt{6}$)	4.39	−0.01
3.041	2.91	321 ($\sqrt{14}$)	2.87	0.04
3.270	2.70	400 ($\sqrt{16}$)	2.69	0.01
3.720	2.38	420 ($\sqrt{20}$)	2.41	−0.03
		421 ($\sqrt{21}$)	2.35	0.03

[a] θ_{obsd} = experimental scattering angles; d_{obsd} = experimental and d_{calcd} = calculated *d* spacing; *hkl* = assigned indices.

tice of micellar cubic phases (Cub_I) occurring in thermotropic systems formed by spheroidic aggregates with soft corona.[20,65c] On the other hand, a *Pm3n* lattice has never been reported for a bicontinuous cubic phase,[17,18,66] hence, it is most likely that the *Pm3n* cubic phases of compounds **3^{n}/*m*** represent micellar cubic phases composed of closed spheroidic aggregates.[65] This assumption is in line with the position of these cubic phases in the phase sequence SmA–Col–Cub_I, as observed upon increasing the number and length of the C-terminal chains. The calculated lattice parameter increases from $a_{cub}=10.4$ nm for compound **3^{14}/2** to $a_{cub}=10.8$ nm for compounds **3^{16}/2** and **3^{16}/3** with longer C-terminal chains. In these cubic phases the molecules are organized in closed spheroidic aggregates and there are 8 of these aggregates in each unit cell that have, depending on their crystallographic position, a slightly different shape (see Figure 1 and 10).[18c,20,21,65] For the compounds under discussion each micelle is built up of approximately 85 molecules (see Table 6, and Table S2 in the Supporting Information). The molecular structure of these cubic phases can be regarded as reverse (type 2) micellar cubic phases, in which spheroids adopt fixed positions on a long-range cubic *Pm3n* lattice in a continuum of the molten alkyl chains provided by the three C-terminal chains (Cub_{I2} phases). The spheroids should have a core–shell structure with an aliphatic core formed by the N-terminal chains in a stratum formed by the charged units, similar to the models shown for the Col_{hex} phases (Figure 8d,e and Figure 10). These core–shell spheroids develop from the Col_{hex} phases by increasing the apolar–polar interface curvature of the core–shell cylinders that is achieved by increasing the length of the C-terminal chains from $n=12$ (Col_{hex}) to $n=16$ (Cub_I; compare compounds **3^{12}/3**, **3^{14}/3**, and **3^{16}/3** in Table 5).[67–69]

It is interesting to note that in the series of compounds **3^{16}/*m*** the columnar phase is limited to a single compound (**3^{16}/4**). Reduction of the length of the N-terminal chain by only one CH_2 group leads to the micellar cubic phase (Cub_I/*Pm3n*), whereas adding only one additional CH_2 gives an SmA phase. This is very surprising and unusual, as the transition between these three completely different types of mesophases with very different interface curvatures usually requires very distinct molecular structures.[18–22,24,25] This is the first example of a series of three directly neighboring homologues that shows a Sm–Col–Cub_I transition. This observation can be explained with the change of the molecular shape from taper to a polycatenar structure (specifically a tetracatenar structure with an unequal distribution of the terminal chains).[70] If the N-terminal chains are short ($m=$ 2–4), then mixing of these chains with the C-terminal chains, though entropically favorable, seems to be energetically unfavorable and hence these chain form their own domains. The segregation of these short alkyl chains from the polar groups leads to spheroidic, columnar, or lamellar aggregates, depending on the curvature imposed on the polar regions by the C-terminal chains at the periphery. However, for longer N-terminal chains ($m>4$) there is not sufficient space in the cores of the spheroidic and cylindrical aggregates, and the mixing of N-terminal and C-terminal chains becomes the energetically and entropically favorable packing mode. It favors the antiparallel side-by side packing of the rods dramatically, which reduces the interfacial curvature between the aromatic/ionic regions and the lipophilic regions, driving the transition from strongly curved spheroidic via columnar to noncurved (lamellar) aggregates.

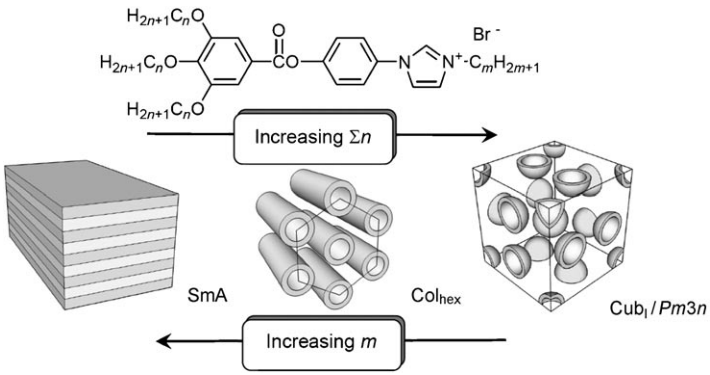

Figure 10. Development of the mesophase structure depending on the length and number of the C-terminal chains and the length of the N-terminal chains attached to the imidazolium-based rodlike aromatic core.

Conclusion

Imidazolium-based ionic LCs constitute a relatively new class of materials in which self-organization and nanoscale segregation are imparted to ionic liquids. The anisometric properties of these materials and the possibility to switch between distinct modes of self-organization[14,30] offer applications of these materials in functional devices, such as in photovoltaics, in fuel cells, batteries, as a templating medium, and as direction-dependent ion-conducting materials.[15b]

Herein we report the first systematic structure–property relationship study of rodlike imidazolium salts focusing on the effects of the number and length of C- and N-terminal chains on the self-assembly into lamellar, columnar, and spheroidic supermolecular aggregates and the modes of the transitions between them.

Using aryl-amination chemistry a series of new ILCs has been prepared wherein the charged imidazolium moiety has been incorporated in the rigid part of rodlike mesogenic cores. By modification of the number and length of the C-terminal chains and the length of the N-terminal chain the molecular shape has been modified from rodlike to taper or polycatenar. The strong electrostatic interactions between the ionic parts lead to a significant mesophase stabilization. For this reason formation of columnar and micellar cubic phases by increasing the number and length of the C-terminal chains was only achieved for the imidazolium salts, whereas for related nonionic imidazoles these structural changes lead to a complete loss of mesogenity. Surprisingly, the length of the N-terminal chain has an unusual strong effect on the self-assembly of the ionic imidazolium-based LCs. Very short chains prefer an end-to-end packing of the mesogens, leading to distinct regions in which the N-terminal chains are organized separately from the C-terminal chains. Elongation of the N-terminal chains allows the mixing of these chains with the C-terminal chains, and this requires a complete intercalation of the aromatic cores. For the single- and double-chain compounds this intercalation gives rise to a transition from bilayer (SmA_2) to monolayer smectic phases. For compounds with three C-terminal chains the end-to-end packing of short N-terminal chains leads to spheroidic and columnar aggregates. In these aggregates the N-terminal alkyl chains form the cores that are enclosed by shells of the polar ionic imidazolium groups and the bromide counterions. These core–shell aggregates form periodic arrays in the lipophilic continuum of the fluid C-terminal chains, resulting in spheroidic cubic phases with *Pm*3*n* symmetry and hexagonal columnar phases with *p*6*mm* symmetry. For these triple-chain compounds, upon elongation of the N-terminal chain, chain mixing and intercalation causes the loss of interfacial curvature and the micellar cubic and columnar phases were replaced by single-layer smectic phases. Due to the strong restriction of the space available for the N-terminal chains in the core–shell aggregates only slight elongation of these chains is sufficient to give dramatic effects. In this way it was possible to achieve the phase sequence Cub_{I2}/*Pm*3*n*–Col_{hex2}/*p*6*mm*–SmA for a series of three directly neighboring homologues differing by only one additional single CH_2 unit from each other. The change of the segregation regime depending on the length of the N-terminal chain is also responsible for the unexpected phase sequence Cub_I–Col–SmA observed upon elongation of the N-terminal chain. This is opposite to the effect of enlarging the number and length of the C-terminal chains, which gives the (usually observed) sequence SmA–Col–Cub_I (Figure 10). Overall, these investigations contribute to the understanding and control of the self-assembly behavior of rodlike ionic liquid crystals.

Acknowledgements

This work was supported by funds from the National Natural Science Foundation of China (no. 20972133), the Ph.D. Programs Foundation of the Education Ministry of China (no. 2007067300), and the Fonds der Chemischen Industrie (Germany). We thank Prof. M. J. Xie and Dr. L. Du for a helpful discussion.

[1] For reviews, see: a) K. R. Seddon, *J. Chem. Technol. Biotechnol.* **1997**, *68*, 351–356; b) T. Welton, *Chem. Rev.* **1999**, *99-99*, 2071–2083; c) P. Wasserscheid, W. Keim, *Angew. Chem.* **2000**, *112*, 3926–3945; *Angew. Chem. Int. Ed.* **2000**, *39*, 3772–3789; d) R. Sheldon, *Chem. Commun.* **2001**, 2399–2407; e) J. Dupont, R. F. de Souza, P. A. Z. Suarez, *Chem. Rev.* **2002**, *102*, 3667–3691; f) A. Corma, H. Garcia, *Chem. Rev.* **2003**, *103*, 4307–4365; g) C. E. Song, *Chem. Commun.* **2004**, 1033–1043; h) R. G. Weiss, *Tetrahedron* **1988**, *44*, 3413–3475; i) H. Kansui, S. Hiraoka, T. Kunieda, *J. Am. Chem. Soc.* **1996**, *118*, 5346–5352.

[2] a) T. Trulove, P. C. Mantz, *Electrochemical Properties of Ionic Liquids. In Ionic Liquids in Synthesis* (Eds.: P. Wasserscheid, T. Welton), Wiley-VCH, Weinheim, **2003**, pp. 103–126; b) *Electrochemical Aspects of Ionic Liquids* (Ed.: H. Ohno), Wiley, New York, **2005**; c) M. C. Buzzeo, R. G. Evans, R. G. Compton, *ChemPhysChem* **2004**, *5*, 1106–1120.

[3] Y. Sanami, M. Funahashi, T. Kato, *J. Am. Chem. Soc.* **2008**, *130*, 13206–13207.

[4] W. Dobbs, J. M. Suisse, L. Douce, R. Welter, *Angew. Chem.* **2006**, *118*, 4285–4288; *Angew. Chem. Int. Ed.* **2006**, *45*, 4179–4182.

[5] a) P. Bonhôte, A. P. Dias, N. Papageorgiou, K. Kalyanasundaram, *Inorg. Chem.* **1996**, *35*, 1168–1178; b) S. A. Forsyth, J. M. Pringle, D. R. MacFarlane, *Aust. J. Chem.* **2004**, *57*, 113–119.

[6] T. Kato, N. Mizoshita, K. Kishimoto, *Angew. Chem.* **2006**, *118*, 44–74; *Angew. Chem. Int. Ed.* **2006**, *45*, 38–68.

[7] *Handbook of Liquid Crystals* (Eds.: D. Demus, J. W. Goodby, G. W. Gray, H.-W. Spiess, V. Vill), Wiley-VCH, Weinheim, **1998**.

[8] I. J. B. Lin, C. S. Vasam, *J. Organomet. Chem.* **2005**, *690*, 3498–3512.

[9] K. Binnemans, *Chem. Rev.* **2005**, *105*, 4148–4204.

[10] N. Yamanaka, R. Kawano, W. Kubo, N. Masaki, T. Kitamura, Y. Wada, M. Watanabe, S. Yanangida, *J. Phys. Chem. B* **2007**, *111*, 4763–4769.

[11] N. Yamanaka, R. Kawano, W. Kubo, T. Kitamura, Y. Wada, M. Watanabe, S. Yanagida, *Chem. Commun.* **2005**, 740–742.

[12] W. Dobbs, B. Heinrich, C. Bourgogne, B. Donnio, E. Terazzi, M.-E. Bonnet, F. Stock, P. Erbacher, A.-L. Bolcato-Bellemin, L. Douce, *J. Am. Chem. Soc.* **2009**, *131*, 13338–13346.

[13] a) S. Sergeyev, W. Pisula, Y. H. Geerts, *Chem. Soc. Rev.* **2007**, *36*, 1902–1929; b) *Liquid Crystalline Functional Assemblies and their Supramolecular Structures, Structure and Bonding* (Eds.: D. M. P. Mingos, T. Kato), Springer, Heidelberg, **2008**.

[14] S. Yazaki, Y. Kamikawa, M. Yoshio, A. Hamasaki, T. Mukai, H. Ohno, T Kato, *Chem. Lett.* **2008**, *37*, 538–539.

[15] a) K. Hoshino, M. Yoshio, T. Mukai, K. Kishimoto, H. Ohno, T. Kato, *J. J. Polym. Sci. Part A* **2003**, *41*, 3486–3492; b) M. Yoshio, T. Mukai, H. Ohno, T. Kato, *J. Am. Chem. Soc.* **2004**, *126*, 994- 995; c) M. Yoshio, T. Kagata, K. Hoshino, T. Mukai, H. Ohno, T. Kato, *J. Am. Chem. Soc.* **2006**, *128*, 5570–5577.

[16] K. Borisch, S. Diele, P. Göring, C. Tschierske, *Chem. Commun.* **1996**, 237–238.

[17] a) S. Diele, *Curr. Opin. Colloid Interface Sci.* **2002**, *7*, 333–342; b) M. Imperor-Clerc, *Curr. Opin. Colloid Interface Sci.* **2005**, *9*, 370–376.

[18] a) K. Borisch, S. Diele, P. Göring, H. Kresse, C. Tschierske, *J. Mater. Chem.* **1998**, *8*, 529–543; b) K. Borisch, S. Diele, P. Göring, H. Müller, C. Tschierske, *Liq. Cryst.* **1997**, *22*, 427–443; c) K. Borisch, S. Diele, P. Göring, H. Kresse, C. Tschierske, *Angew. Chem.* **1997**, *109*, 2188–2190; *Angew. Chem. Int. Ed. Engl.* **1997**, *36*, 2087–2089; d) K. Borisch, C. Tschierske, P. Göring, S. Diele, *Chem. Commun.* **1998**, 2711–2712; e) K. Borisch, C. Tschierske, P. Göring, S. Diele,

Langmuir **2000**, *16*, 6701–6708; f) P. Fuchs, C. Tschierske, K. Raith, K. Das, S. Diele, *Angew. Chem.* **2002**, *114*, 650–653; *Angew. Chem. Int. Ed.* **2002**, *41*, 628–631.
[19] T. Kato, T. Matsuoka, M. Nishii, Y. Kamikawa, K. Kanie, T. Nishimura, E. Yashima, S. Ujiie, *Angew. Chem.* **2004**, *116*, 2003–2006; *Angew. Chem. Int. Ed.* **2004**, *43*, 1969–1972.
[20] G. Ungar, X. Zeng, *Soft Mater.* **2005**, *1*, 95–106.
[21] a) S. D. Hudson, H.-T. Jung, V. Percec, W.-D. Cho, G. Johansson, G. Ungar, V. S. K. Balagurusamy, *Science* **1997**, *278*, 449–452; b) V. Percec, W.-D. Cho, P. E. Mosier, G. Ungar, D. J. P. Yeardley, *J. Am. Chem. Soc.* **1998**, *120*, 11061–11070; c) V. Percec, M. N. Holerca, S. Uchida, W.-D. Cho, G. Ungar, Y.-S. Lee, D. J. P. Yeardley, *Chem. Eur. J.* **2002**, *8*, 1106–1117; d) D. J. P. Yeardley, G. Ungar, V. Percec, M. N. Holerca, G. Johansson, *J. Am. Chem. Soc.* **2000**, *122*, 1684–1689; e) B. M. Rosen, C. J. Wilson, D. A. Wilson, M. Peterca, M. R. Imam, V. Percec, *Chem. Rev.* **2009**, *109*, 6275–6540.
[22] a) X. H. Cheng, S. Diele, C. Tschierske, *Angew. Chem.* **2000**, *112*, 605–608; *Angew. Chem. Int. Ed.* **2000**, *39*, 592–595; b) X. H. Cheng, M. K. Das, S. Diele, C. Tschierske, *Langmuir* **2002**, *18*, 6521–6529.
[23] M. Lee, B.-K. Cho, H. Kim, W.-C. Zin, *Angew. Chem.* **1998**, *110*, 661–663; *Angew. Chem. Int. Ed.* **1998**, *37*, 638–640.
[24] a) T. Noguchia, K. Kishikawab, S. Kohmotob, *Liq. Cryst.* **2008**, *35*, 1043–1050; b) X. L. Zhou, T. Narayanan, Q. Li, *Liq. Cryst.* **2007**, *34*, 1243–1248; c) B.-K. Cho, A. Jain, S. M. Gruner, U. Wiesner, *Science* **2004**, *305*, 1598–1601; d) T. Kato, T. Matsuoka, M. Nishii, Y. Kamikawa, K. Kanie, T. Nishimura, E. Yashima, S. Ujiie, *Angew. Chem.* **2004**, *116*, 2003–2006; *Angew. Chem. Int. Ed.* **2004**, *43*, 1969–1972; e) A. Kohlmeier, D. Janietz, S. Diele, *Chem. Mater.* **2006**, *18*, 1483–1489; f) M. Lehmann, M. Jahr, *Chem. Mater.* **2008**, *20*, 5453–5456; g) S. Coco, C. Cordovilla, B. Donnio, P. Espinet, M. J. Garcia-Casas, D. Guillon, *Chem. Eur. J.* **2008**, *14*, 3544–3552.
[25] a) C. Tschierske, *J. Mater. Chem.* **2001**, *11*, 2647–2671; b) C. Tschierske, *Ann. Rep. Progr. Chem. Sect. C* **2001**, *97*, 191–267.
[26] M. R. Imam, M. Peterca, U. Edlund, V. S. K. Balagurusamy, V. Percec, *J. J. Polym Sci. Part A* **2009**, *47*, 4165–4193.
[27] C. K. Lee, H. W. Huang, I. J. B. Lin, *Chem. Commun.* **2000**, 1911–1912.
[28] M. Tosoni, S. Laschat, A. Baro, *Helv. Chim. Acta* **2004**, *87*, 2742–2749.
[29] Y. R. Zhao, X. Chen, X. D. Wang, *J. Phys. Chem. B* **2009**, *113*, 2024–2030.
[30] M. Yoshio, T. Mukai, K. Kanie, M. Yoshizawa, H. Ohno, T. Kato, *Chem. Lett.* **2002**, 320–321.
[31] W. Dobbs, D. Laurent, *New J. Chem.* **2006**, *30*, 528–532.
[32] M. Yoshio, T. Ichikawa, H. Shimura, T. Kagata, A. Hamasaki, T. Mukai, H, Ohno, T. Kato, *Bull. Chem. Soc. Jpn.* **2007**, *80*, 1836–1841.
[33] J. H. Olivier, F. Camerel, J. Barbera, P. Retailleau, R. Ziessel, *Chem. Eur. J.* **2009**, *15*, 8163–8174.
[34] H. Shimura, M. Yoshio, K. Hoshino, T. Mukai, H. Ohno, T. Kato, *J. Am. Chem. Soc.* **2008**, *130*, 1759–1765.
[35] C. O. Osuji, C. Y. Chao, C. K. Ober, E. L. Thomas, *Macromolecules* **2006**, *39*, 3114–3117.
[36] K. Goossens, P. Nockemann, K. Driesen, K. Driesen, B. Goderis, C. Görller-Walrand, K. V. Hecke, L. V. Meervelt, E. Pouzet, K. Binnemans, T. Cardinaels, *Chem. Mater.* **2008**, *20*, 157–168.
[37] Q. X. Zhang, L. S. Jiao, C. S. Shan, P. Hou, B. Chen, X. Y. Xu, L. Niu, *Liq. Cryst.* **2008**, *35*, 765–772.
[38] Q. X. Zhang, C. S. Shan, X. D. Wang, L. L. Chen, L. Niu, B. Chen, *Liq. Cryst.* **2008**, *35*, 1299–1305.
[39] H. Yoshizawa, T. Mihara, N. Koide, *Liq. Cryst.* **2005**, *32*, 143–149.
[40] J. Fouchet, L. Douce, B. Heinrich, R. Welter, A. Louati, *Beilstein J. Org. Chem.* **2009**, *5*, 51.
[41] L. Cui, L. Zhu, *Liq. Cryst.* **2006**, *33*, 811–818.
[42] B. El Hamaoui, L. J. Zhi, W. Pisula, U. Kolb, J. Wu, K. Müllen, *Chem. Commun.* **2007**, 2384–2386.
[43] J. Motoyanagi, T. Fukushima, T. Aida, *Chem. Commun.* **2004**, 101–103.
[44] a) S. Kumar, K. S. Pal, *Tetrahedron Lett.* **2005**, *46*, 2607–2610; b) K. S. Pal, S. Kumar, *Tetrahedron Lett.* **2006**, *47*, 8993–8997.
[45] A bicontinuous cubic phase was recently reported for a triphenylene-based disclike molecule with six imidazolium units: M. A. Alam, J. Motoyanagi, Y. Yamamoto, T. Fukushima, J. Kim, K. Kato, M. Takata, A. Saeki, S. Seki, S. Tagawa, T. Aida, *J. Am. Chem. Soc.* **2009**, *131*, 17722–17723.
[46] a) D. Navarro-Rodriguez, Y. Frere, P. Gramain, D. Guillon, A. Skoulios, *Liq. Cryst.* **1991**, *9*, 321–335; b) L. Cui, V. Sapagovas, G. Lattermann, *Liq. Cryst.* **2002**, *29*, 1121–1132; c) H. Yoshizawa, T. Mihara, N. Koide, *Mol. Cryst. Liq. Cryst.* **2004**, *423*, 61–72.
[47] a) C. J. Bowlas, D. W. Bruce, K. R. Seddon, *Chem. Commun.* **1996**, 1625–1626; b) C. M. Gordon, J. D. Holbrey, A. R. Kennedy, K. R. Seddon, *J. Mater. Chem.* **1998**, *8*, 2627–2636; c) J. D. Holbrey, K. R. Seddon, *J. Chem. Soc. Dalton Trans.* **1999**, 2133–2139; d) G. A. Knight, B. D. Shaw, *J. Chem. Soc.* **1938**, 682–683; e) E. J. R. Sudholter, J. B. F. N. Engberts, W. H. De Jeu, *J. Phys. Chem.* **1982**, *86*, 1908–1913.
[48] J. M. Suisse, S. Bellemin-Laponnaz, L. Douce, A. Maisse-Francois, R. Welter, *Tetrahedron Lett.* **2005**, *46*, 4303–4305.
[49] J. M. Suisse, L. Douce, S. Bellemin-Laponnaz, A. Maisse-François, R. Welter, Y. Miyake, Y. Shimizu, *Eur. J. Inorg. Chem.* **2007**, 3899–3905.
[50] X. J. Li, D. W. Bruce, J. M. Shreeve, *J. Mater. Chem.* **2009**, *19*, 8232–8238.
[51] P. H. J. Kouwer, T. M. Swager, *J. Am. Chem. Soc.* **2007**, *129*, 14042–14052.
[52] a) S. H. Seo, J. H. Park, G. N. Tew, J. Y. Chang, *Tetrahedron Lett.* **2007**, *48*, 6839–6844; b) S. H. Seo, J. H. Park, J. Y. Chang, *Langmuir* **2009**, *25*, 8439–8441.
[53] S. H. Seo, G. N. Tew, J. Y. Chang, *Soft Matter* **2006**, *2*, 886–891.
[54] Compounds related to **1^{12}/3** and **1^{12}/12** but with I^- and BF_4^- counterions were reported previously (see the Supporting Information of ref. [51]). Compared with the bromides **1^{12}/3** and **1^{12}/12**, the corresponding iodides have higher melting points and similar clearing temperatures, therefore narrower mesophase ranges are formed by the iodides, whereas the corresponding tetrafluoroborates have lower melting temperature and similar clearing temperatures, therefore showing broader mesophase ranges than the bromides.
[55] Compound **1^{12}/0** was previously reported (Cr 102 °C SmA 130 °C Iso) in ref. [51].
[56] a) P. E. Fanta, *Chem. Rev.* **1964**, *64*, 613–632; b) T. Yamamoto, Y. Kurata, *Can. J. Chem.* **1983**, *61*, 86–86; c) J. Lindley, *Tetrahedron Lett.* **1984**, *40*, 1433–1456; d) J. Fouchet, L. Douce, B. Heinrich, R. Welter, A. Louati, *Beilstein J. Org. Chem.* **2009**, *5*, 51.
[57] K. Hwang, S. Park, *Synth. Commun.* **1993**, *23*, 2845–2849.
[58] *Textures of Liquid Crystals* (Ed. I. Dierking), Wiley-VCH, Weinheim, **2003**.
[59] The molecular length L was determined with space-filling models (also known as calotte models or CPK models by Corey, Pauling, and Koltun), see: R. B. Corey, L. Pauling, *Rev. Sci. Instrum.* **1953**, *24*, 621–627.
[60] Herein this type of intercalated bilayer structure is assigned as SmA_2 although the d parameter is significantly smaller than $d=2L$ and corresponds to $L<d<2L$, which is usually assigned to double-layer smectic phases abbreviated as SmA_b; in SmA_b phases there is an interdigitation of the rodlike aromatic cores leading to the reduction of d to a value smaller than $2L$; however, in the SmA_2 phases reported here, the aromatic parts adopt a nonintercalated antiparallel end-to-end organization typical for SmA_2 phases; the reduction of the d value is in this case due to the intercalation of the alkyl chains, which retain the end-to-end packing of the rodlike cores and therefore, we prefer to assign these phases as SmA_2.
[61] The structures were solved and refined on F by using the SHELXS-97 program: G. M. Sheldrick, University of Göttingen, Göttingen, **1997**. CCDC-753575 (**1^{10}/0**) and -753576 (**1^{12}/0**) contain the supplementary crystallographic data for this paper. These data can be obtained free of charge from The Cambridge Crystallographic Data Centre via www.ccdc.cam.ac.uk/data_request/cif: a) Crystal data for

1[10]/0: $C_{26}H_{32}N_2O_3$; triclinic; space group $P\bar{1}$; $Z=2$; $a=6.938(4)$, $b=12.758(8)$, $c=13.766(9)$ Å; $\alpha=85.627(9)$, $\beta=81.205(9)$, $\gamma=81.976(9)°$; $V=1190.5(13)$ Å^3; $\rho_{calcd}=1.173$ mg m^{-3}; absorption coefficient $=0.077$ mm^{-1}; $T=298$ K; data collection: Bruker Smart ApexII; θ range for data collection: 1.50 to 28.40°; 10354 reflections and 5407 with $(I>2\sigma(I))$; maximum residual electron density 0.15 e Å^{-3}; $R_1=0.078$, $R_{w2}=0.14$; b) Crystal data for **1[12]/0**: $C_{28}H_{38}N_2O_3$; triclinic; space group $P\bar{1}$; $Z=2$; $a=6.988(5)$, $b=12.565(5)$, $c=15.054(5)$ Å; $\alpha=80.395(5)5$, $\beta=83.604(5)$, $\gamma=81.783(5)°$; $V=1284.7(11)$ Å^3; $\rho_{calcd}=1.160$ mg m^{-3}; absorption coefficient $=0.075$ mm^{-1}; $T=293$ K; data collection: Bruker Smart 1000; θ range for data collection: 1.66 to 28.48°; 12341 reflections and 10493 with $(I>2\sigma(I))$; maximum residual electron density 0.14 e Å^{-3}; $R_1=0.0822$, $R_{w2}=0.19$.

[62] An additional texture is shown in Figure S13a in the Supporting Information.

[63] For compound **3[16]/4** only a single reflection was observed in the powder XRD pattern (see Figure S22 in the Supporting Information), but the 2D diffraction pattern of an aligned sample (see Figure S21 in the Supporting Information) confirms a hexagonal lattice.

[64] In the case of compound **3[14]/3** the cubic mesophase is only formed upon cooling from the isotropic liquid state, whereas upon heating from the crystalline state a hexagonal columnar phase was observed. Remarkably the Col–Iso transition is 18 K higher than the temperature at which the cubic phase appears on cooling.

[65] a) K. Fontell, K. K. Fox, E. Hansson, *Mol. Cryst. Liq. Cryst. Lett. Sect.* **1985**, *1*, 9–17; b) K. Fontell, *Colloid Polym. Sci.* **1990**, *268*, 264–285; c) P. Ziherl, R. D. Kamien, *J. Phys. Chem. B* **2001**, *105*, 10147–10158; d) G. M. Grason, B. A. DiDonna, R. D. Kamien, *Phys. Rev. Lett.* **2003**, *91*, 058304; e) J. Charvolin, J. F. Sadoc, *J. Phys.* **1988**, *49*, 521–526; f) R. Vargas, P. Mariani, A. Gulik, V. Luzzati, *J. Mol. Biol.* **1992**, *225*, 137–145.

[66] S. T. Hyde in *Handbook of Applied Surface and Colloid Chemistry* (Ed.: K. Holmberg), Wiley, New York, **2001**, pp. 299.

[67] Core–shell structures were found for columnar and spheroidic aggregates formed by taper-shaped dendritic molecules with a peptide-based apex; however, for these structures hollow channel and hollow sphere structures were proposed: a) V. Percec, A. E. Dulcey, V. S. K. Balagurusamy, Y. Miura, J. Smidrkal, M. Peterca, S. Nummelin, U. Edlund, S. D. Hudson, P. A. Heiney, H. Duan, S. N. Magonov, S. A. Vinogradov, *Nature* **2004**, *430*, 764–768; b) M. Peterca, V. Percec, A. E. Dulcey, S. Nummelin, S. Korey, M. Ilies, P. A. Heiney, *J. Am. Chem. Soc.* **2006**, *128*, 6713–6720; c) V. Percec, A. E. Dulcey, M. Peterca, P. Adelman, R. Samant, V. S. K. Balagurusamy, P. A. Heiney, *J. Am. Chem. Soc.* **2007**, *129*, 5992–6002; d) V. Percec, M. Peterca, A. E. Dulcey, M. R. Imam, S. D. Hudson, S. Nummelin, P. Adelman, P. A. Heiney, *J. Am. Chem. Soc.* **2008**, *130*, 13079–13094.

[68] a) V. Percec, M. Glodde, M. Peterca, A. Rapp, I. Schnell, H. W. Spiess, T. K. Bera, Y. Miura, V. S. K. Balagurusamy, E. Aqad, P. A. Heiney, *Chem. Eur. J.* **2006**, *12*, 6298–6314; b) L. Gehringer, C. Bourgogne, D. Guillon, B. Donnio, *J. Am. Chem. Soc.* **2004**, *126*, 3856–3867; c) A. Schaz, G. Lattermann, *Liq. Cryst.* **2005**, *32*, 407–415; d) M. Prehm, F. Liu, U. Baumeister, X. B. Zeng, G. Ungar, C. Tschierske, *Angew. Chem.* **2007**, *119*, 8118; *Angew. Chem. Int. Ed.* **2007**, *46*, 7972–7975.

[69] Core–shell structures are quite common for morphologies of block copolymers: a) I. W. Hamley, *The Physics of Block Copolymers*, Oxford University Press, Oxford, **1998**; b) V. Abetz, P. F. W. Simon, *Adv. Polym. Sci.* **2005**, *189*, 125–212.

[70] All reported cubic phases of polycatenar compounds are of the bicontinuous type: a) J. Malthete, H. T. Nguyen, C. Destrade, *Liq. Cryst.* **1993**, *13*, 171–187; b) H.-T. Nguyen, C. Destrade, J. Malthete, *Adv. Mater.* **1997**, *9*, 375–388; c) M. Gharbia, A. Gharbi, H. T. Nguyen, J. Malthete, *Curr. Opin. Colloid Interface Sci.* **2002**, *7*, 312–325; d) D. W. Bruce, *Acc. Chem. Res.* **2000**, *33*, 831–840; e) X. B. Zeng, L. Cseh, G. H. Mehl, G. Ungar, *J. Mater. Chem.* **2008**, *18*, 2953–2961.

Received: November 23, 2009
Published online: March 16, 2010

